Chemie
Ingenieur
Technik

Research Article

Online in color, print in grayscale unless the author(s) contribute to the cost
These are not the final page numbers! ↘↘

1

Impact of Hard Magnetic Nanocrystals on the Properties of Hardened Cement Paste

Patrick A. Kißling, Markus Mahlbacher, Christoph Wesemann, Alexander Mundstock, Franziska Lübkemann-Warwas, Stephen Klimke, Franz Renz, Ludger Lohaus, Michael Haist, and Nadja C. Bigall*

Supporting Information available online

In this work, nano-sized hard magnetic gallium-substituted iron oxide crystals, wherein gallium is used to stabilize the metastable epsilon iron oxide phase, were added to cement-water suspensions at different ratios, which were subsequently hydrated for at least 28 days. It is shown that higher contents of such nanocrystals in the hardened cement paste introduce a magnetic moment, whereas the mechanical properties remain unchanged compared to non-blended hardened cement paste for a wide concentration range.

1 Introduction

In our modern society, the most common building material is concrete [1], which is made from coarse and fine aggregates (e.g., sand, gravel, or crushed stones), Portland cement (in this case CEM I 42.5 R), water, and various admixtures. Cement itself mainly consists of Ca_3SiO_5, Ca_2SiO_4, and $Ca_3Al_2O_6$ and acts as the binder or glue of the composite material [2]. Over time, the requirements of building materials change as extrinsic factors like climate, resource scarcity, and politics rise up, with adaptions of the composite system becoming necessary [3]. Most approaches to modify the properties of cementitious suspensions, hydrated cement, and hardened cement paste, work on the macroscopic or microscopic level, e.g., by adding fillers such as sand or quartz powder to increase packing density and reduce the amount of binder or superplasticizer to improve fluidity and pumpability of concrete [4–13]. Alternatively, nano-scaled additives (TiO_2 [14, 15], ZnO [15, 16], carbon nanotubes [17, 18], α-Fe_2O_3 [19–22], SiO_2 [21–27], and tobermorite nanofibers [28]), can be incorporated. This leads to enhanced external compression and tensile strength [15, 23], a reduction of the dormant period while accelerating the hydration of cement, as well as lowering the initial and final setting time by 90–100 min [23], respectively. Hereby, specific modifications are observed on the paste level already, without additional aggregates.

Previously, Ohkoshi et al. [29] synthesized hard-magnetic ε-Fe_2O_3 nanocrystals (NCs) demonstrating their capability to absorb millimeter waves due to a high coercive field H_c. They showed that the partial substitution of iron atoms by gallium stabilizes the metastable phase of ε-Fe_2O_3 and changes coercive field H_c as a function of the substitution rate, changing the absorption wavelength or rather the resonance frequency f_r as follows by

$$f_r \approx \frac{\gamma}{2\pi\sqrt{1-A^2}} \sqrt{4\pi M_s(H_a + 4\pi E\, M_s)} \tag{1}$$

where γ corresponds to the gyromagnetic ratio of an electron ($1.76 \cdot 10^{11}$ $T^{-1}s^{-1}$) [30], A to the damping constant, H_a

[1,2]Patrick A. Kißling https://orcid.org/0000-0001-5596-9976,
[2]Markus Mahlbacher, [1]Christoph Wesemann,
[1]Dr. rer. nat. Alexander Mundstock, [1]Dr. rer. nat. Franziska Lübkemann-Warwas, [3]Dr. rer. nat. Stephen Klimke,
[3,4]Prof. Dr. rer. nat. Franz Renz, [2]Prof. Dr.-Ing. Ludger Lohaus, [2]Prof. Dr.-Ing. Michael Haist, [1,4]Prof. Dr. rer. nat. Nadja C. Bigall
https://orcid.org/0000-0003-0171-1106
(nadja.bigall@pci.uni-hannover.de)

[1]Leibniz University Hannover, Institute of Physical Chemistry and Electrochemistry, Callinstr. 3a, 30167 Hanover, Germany.

[2]Leibniz University Hannover, Institute of Building Materials Science, Appelstraße 9a, 30167 Hanover, Germany.

[3]Leibniz University Hannover, Institute of Inorganic Chemistry, Callinstraße 3–9, 30167 Hanover, Germany.

[4]Leibniz University Hannover, Laboratory of Nano and Quantum Engineering (LNQE), Schneiderberg 39, 30167 Hanover, Germany.

Online in color, print in grayscale unless the author(s) contribute to the costs.
✓✓ These are not the final page numbers!

2

Research Article

Chemie
Ingenieur
Technik

to the uniaxial anisotropy field of an unpatterned film, E to the effective demagnetization factor, and $4\pi M_s$ to the saturation magnetization according to Kittel (1) [31].

In the present work, these new magnetic properties are induced into hardened cement paste. By doing so, the general properties, such as porosity and compressive strength should be maintained or improved.

The crux of the matter being whether the magnetic properties of the NCs stay the same in this matrix is answered by evaluating the magnetic properties. We investigate which structure-properties hardened cement pastes blended or functionalized with $Ga_{0.043}Fe_{1.957}O_3$ nanomagnets exhibit compared to non-blended hardened cement paste. To better quantify these aspects, aggregates and other additives, such as sand or slag, were neglected and only the change in the properties of hardened cement paste cuboids were studied, which for example showed a tremendous increase of magnetic remanence M_R by a factor of about 750. Here, different amounts (≤ 10 wt %, namely 0, 1, 5, and 10 wt %) of self-synthesized $Ga:Fe_2O_3$ (85 % ε and 15 % α) NCs were added to CEM I 42.5 R (Fig. 1), which already contains 2–5 wt % Fe_2O_3 present as part of brownmillerite (C_4AF) (Fig. S1b in the Supporting Information SI). The blending values were chosen to be comparable to previous studies [14–16, 21–27].

2 Experimental

The experimental details (Sect. S1) as well as the characterization (Sect. S2.1) of all educts and intermediates (where necessary) can be found in Supporting Information SI. Characterization of the as-synthesized NCs by Mössbauer spectroscopy, superconducting quantum interference device (SQUID), powder X-ray diffraction (XRD) reveals the presence of two $Ga:Fe_2O_3$ phases (85 % ε and 15 % α) and from TEM micrographs (Fig. 2a) it can be observed that $Ga:Fe_2O_3$ NCs were polydisperse with a size of 22 nm ± 11 nm. For a detailed characterization see SI Sect. S2.1.2.

3 Results and Discussion

The evaluation of the hardened cement paste samples is divided into two distinct topics: (1) The structural characterization split into the analysis of the chemical composition and morphological appearance and (2) the investigation of mechanical and magnetic properties.

3.1 Structural Characterization

For the chemical composition analysis of hardened cement paste cuboids with an admixture of $Ga:Fe_2O_3$ NCs (≤ 10 wt %, namely 0, 1, 5 and 10 wt %), XRD, thermal

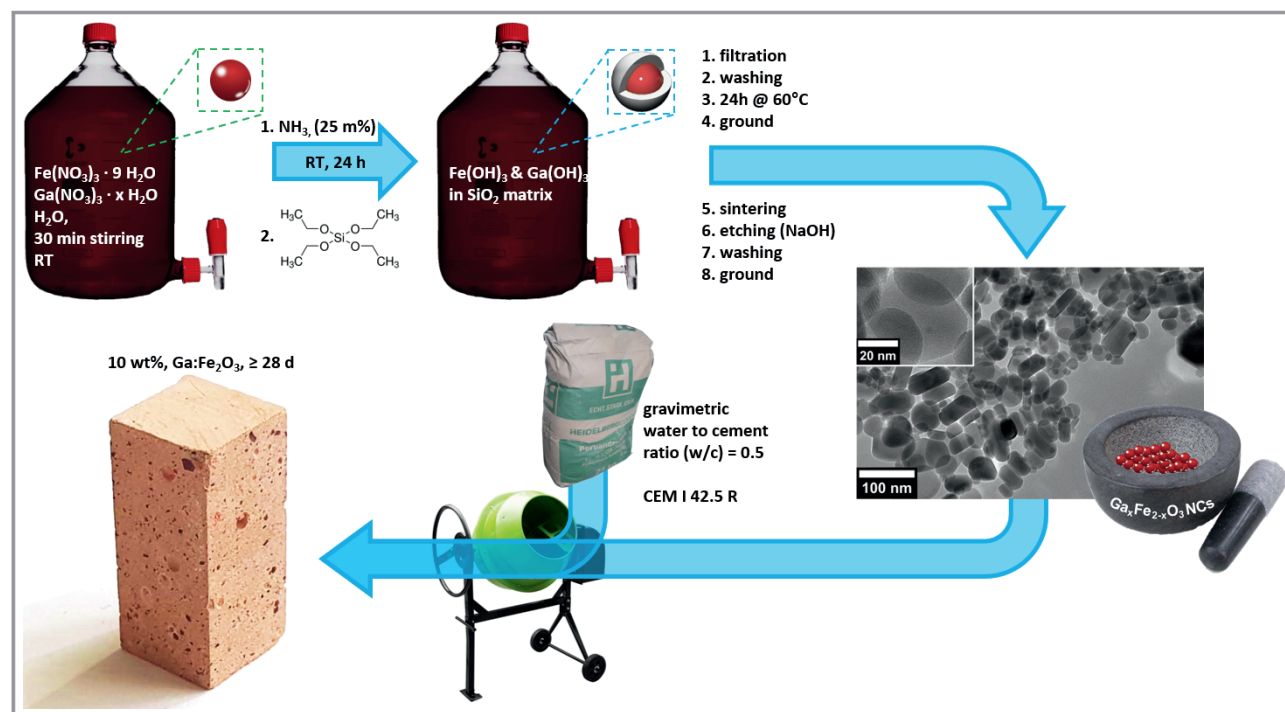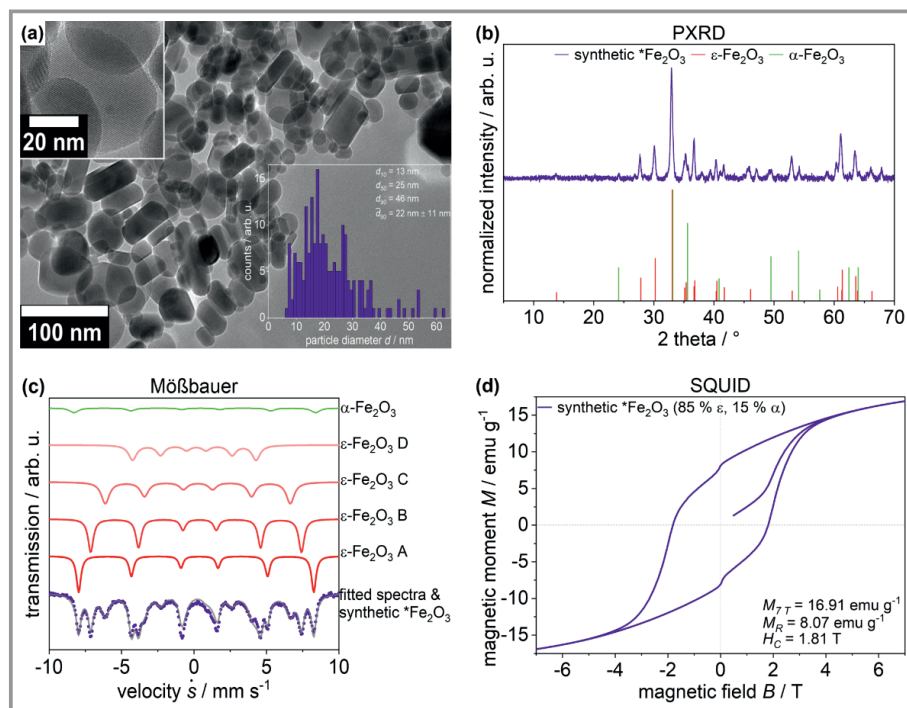**Figure 1.** Schematic illustration of the synthetic pathway and preparation of Ga:Fe₂O₃ NCs, blending of CEM I 42.5 R with a gravimetric water-to-cement ratio (w/c) of 0.5 with Ga:Fe₂O₃ NCs, preparation of hardened cement paste cuboids.

Chemie Ingenieur Technik

Research Article

Online in color, print in grayscale unless the author(s) contribute to the costs.
These are not the final page numbers! ↘↘

3

Figure 2. Evaluation of synthesized NCs. a) TEM micrograph with PSD and zoom-in as insets, b) PXRD pattern including reference patterns of ε-Fe$_2$O$_3$ and α-Fe$_2$O$_3$ [32], c) Mössbauer spectroscopy showing the fitted spectra including five sextets, one of α-Fe$_2$O$_3$ and four of ε-Fe$_2$O$_3$ (A to D), and d) SQUID including maximal magnetization at $B = 7$ T $M_{7\,T}$, remanence M_R, and coercive field H_C.

tion (Fig. 4a and S5a–c in SI), and mercury intrusion porosimetry (Fig. 4b and S5d in SI). In the case of building materials, such knowledge is of utmost importance, since the porosity influences the mass transport, strength, durability, and thermal properties. A higher porosity could lead to less strength as well as higher mass and lower thermal transport and durability of concrete. The evaluation of nitrogen physisorption of all investigated samples presents no significant deviation in terms of the specific surface area (80 to 83 m^{2}g^{-1}) and specific volume (100 to 120 mm^{3}g^{-1}). The mean pore diameter $\bar{d}_{pore}$ shows enlarged pores by up to 28 % in comparison to pure hardened cement paste and 15 % to anhydrous cement with the addition of Ga:Fe$_2$O$_3$ NCs with increasing proportion. The isotherms (Fig. S5c in SI) exhibit H4-type hysteresis loops for all mass fractions with a strong decrease of the desorption branch in the

gravimetric analysis (TGA), and scanning electron microscopy coupled with energy dispersive X-ray spectroscopy (SEM-EDXS) were used. While the first two techniques (PXRD and TGA) show only slight deviations concerning the impact of different amounts of Ga:Fe$_2$O$_3$ NCs on the hydration products (see SI Figs. S2 and S3). SEM-EDXS enabled the spatially resolved validation of the Ga:Fe$_2$O$_3$ NCs distribution in the hardened cement paste blocks (10 mm × 4 mm × 1 mm) (Fig. 3 and S4 in SI). The micrographs exhibit a non-aggregated homogenous distribution in all samples, with the number of Fe fractions increasing with a higher mass fraction of Ga:Fe$_2$O$_3$ NCs, which qualitatively indicates an increasing Fe content in the samples. Significant deviations from the morphology cannot be detected, as the surface of all samples shows almost evenly distributed hydration products in form of flower-like portlandite, while the recorded oxygen values differ between the samples (Fig. S4 in SI), possibly induced by the oxygen of Ga:Fe$_2$O$_3$ NCs.

After showing the impact of the incorporated Ga:Fe$_2$O$_3$ NCs on the chemical composition, the pore structure of the hardened cement paste blocks was investigated via nitrogen physisorp-
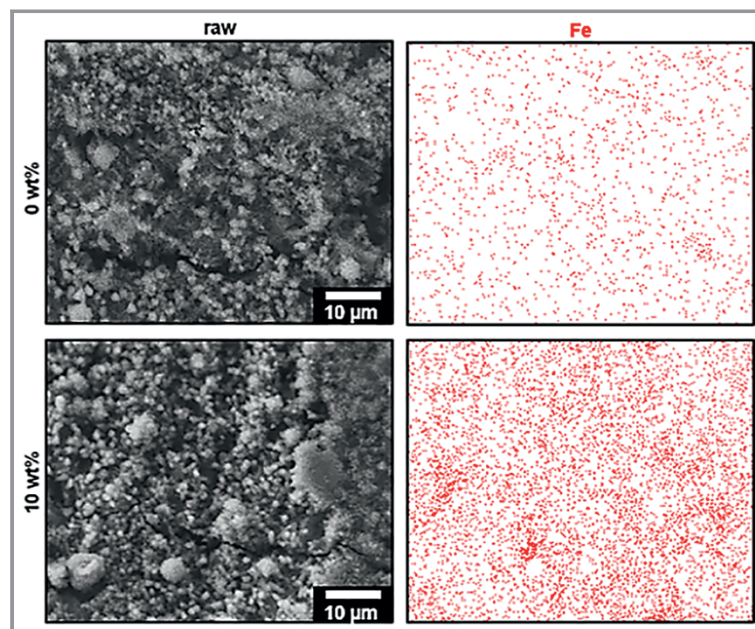

Figure 3. SEM-EDXS data of hardened cement pastes made from anhydrous cement mixed with different mass fractions of Ga:Fe$_2$O$_3$ NCs ($\leq$ 10 wt %, namely 0, 1, 5, and 10 wt %); exemplary shown for non-blended hardened cement paste (0 wt %) and highest amount of Fe$_2$O$_3$ NCs (10 wt %); depicted are (left) micrograph and (right) Fe spots (red).
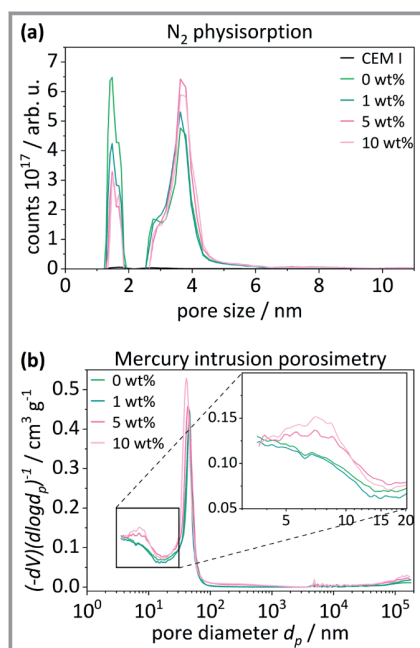
Online in color, print in grayscale unless the author(s) contribute to the costs.
✓✓ **These are not the final page numbers!**

4

Research Article | Chemie Ingenieur Technik

Figure 4. Evaluation of hardened cement paste s of anhydrous cement mixed with different mass fractions of Ga:Fe$_2$O$_3$ NCs; pore size distribution derived from a) nitrogen physisorption and b) mercury intrusion porosimetry.

range of $0.4 \leq p/p_0 \leq 0.5$, as expected when using a wetting adsorbate such as nitrogen [33].

Furthermore, the H4-type hysteresis' shape indicates non-rigid aggregated crystals and not completely filled voids with pore condensate. With a mass fraction of 1, 5, and 10 wt % Ga:Fe$_2$O$_3$ NCs the hysteresis width is increased by 8.5 %, 17 %, and by 12 % compared to the reference composition of 0 wt %. This indicates a change in the pore structure to a higher amount of pores. Simultaneously less completely filled pores, resulting in a decreasing density, which was calculated via weight and volume of the hardened cement paste blocks, of 1.85, 1.79, 1.76, and 1.70 g cm^{-3} with an increasing amount of filler, is observed (see Sect. S1.2.11 in SI). This phenomenon is most probably due to a high concentration of water around Ga:Fe$_2$O$_3$ NCs, because of the high surface-to-volume ratio of nanoparticles [34], during the early solidification process. Similar effects are observed in mercury intrusion porosimetry, with samples showing increasing porosity with increasing Ga:Fe$_2$O$_3$ NCs content, visible in the specific intrusion volume (Fig. S5d in SI) for the low ($p \leq 3.45$ bar) and high-pressure range ($p \leq 4000$ bar). Utilizing the Washburn equation [35] and analysis procedure according to DIN ISO 15901-1:2019-03 [36], this corresponds to larger pore volumes at two ranges of pore diameter d_{pore}, 5–15 nm (Fig. 4b inset) and 50–200 µm (Fig. 4b). Both methods indicate that the porosity or the number of pores increases with rising Ga:Fe$_2$O$_3$ content, both at the nano- and microscale.

The changes of porosity induced by the hydration products formed, which in turn were influenced by the amount

of admixed Ga:Fe$_2$O$_3$ NCs and evaluated via PXRD and TGA, led to a variance in the pore size distribution and density of the samples.

3.2 Investigation of Mechanical and Magnetic Properties

Due to both, the observed increased porosity detected by nitrogen physisorption and mercury intrusion porosimetry as well as the influence of Ga:Fe$_2$O$_3$ NCs, the mechanical and magnetic properties are assumed to change accordingly. Therefore, the mechanical properties were determined by compressive strength test as well as micro- and nanoindentation, and the magnetic properties by SQUID measurements.

3.2.1 Mechanical Properties

The strength of hardened cement paste cubes (40 mm) was examined via a compressive strength test derived from DIN EN 12390-3:2019-10 [37] after 28 d of hydration (Fig. 5). It can be seen that increasing the share of NCs lowers the characteristic compressive strength f_{ck} by up to 28 %, while the change due to 1 wt % is marginal (–1.9 %). At a content of 10 wt % Ga:Fe$_2$O$_3$ NCs, the compressive strength f_{ck} decreases below $f_{ck} = 39.4$ N mm^{-2}, which has to be considered for the application in construction as a building material, but is negligible in regards to non-structural coatings for e.g. tap-proofness [38]. The lowered compressive strength f_{ck} could be due to the enhanced porosity, see calculated density in the previous section as well as the pore volumes in nitrogen physisorption and mercury intrusion porosimetry, caused by the admixture of Ga:Fe$_2$O$_3$ NCs. In addition to this macroscopic investigation, the hardness and stiffness of hardened cement paste on the micro- and nanoscale were determined from micro- and nanoindentation tests (Fig. 6). Force-displacement curves of a Berkovich (nano) and Vickers (micro) indenter are measured and analyzed for indentation hardness H_{IT} and modulus M_{IT} [39].
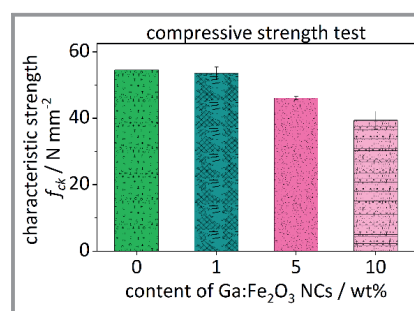

Figure 5. Evaluation of mechanical properties of hardened cement pastes mixed with different mass fractions of Ga:Fe$_2$O$_3$ NCs by compressive strength test at 28 d.

While a clear trend is distinguishable in compressive strength f_{ck}, the micro indentation hardness H_{IT} and modu-
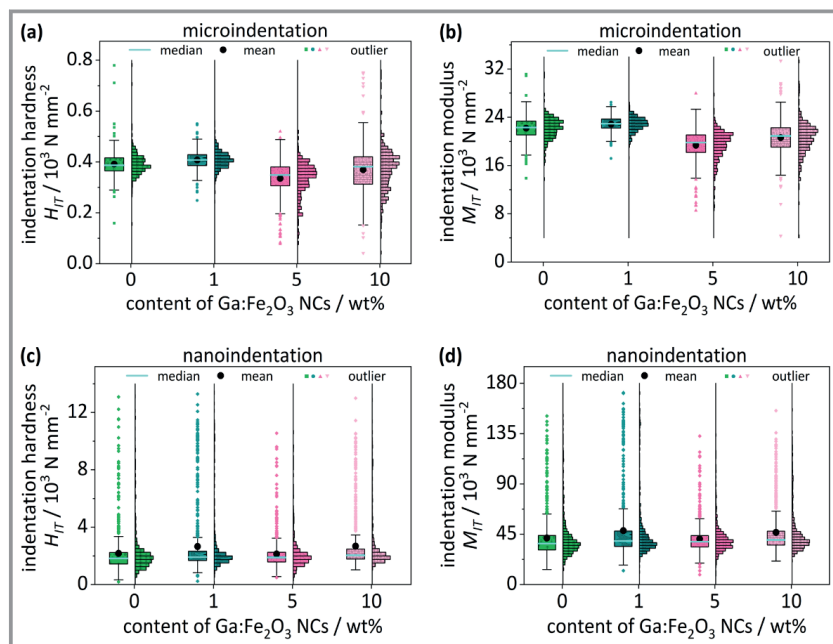
Online in color, print in grayscale unless the author(s) contribute to the costs.
These are not the final page numbers! ↘↘

Chemie Ingenieur Technik Research Article

5

Figure 6. Evaluation of mechanical properties of hardened cement pastes mixed with different mass fractions of Ga:Fe$_2$O$_3$ NCs by indentation hardness H_{IT} derived from a) microindentations and b) nanoindentation as well as indentation modulus H_{IT} derived from c) microindentation and d) nanoindentation.

The pure hardened cement paste (0 wt %, Fig. 7) showed a non-linear curve progression up to $B \cong 0.3$ T, which we attribute to unreacted ferrimagnetic calcium aluminum ferrite (brownmillerite, C$_4$AF) [40] contained in anhydrous CEM I 42.5 R [41], as a fully hydrated cementitious suspension would show no ferromagnetic signal during SQUID measurements [42]. A further increase of $\vec{H}$ leads to a linear curve progression, which was assigned to the paramagnetic materials of hydrated cement. Although no magnetic saturation was observed, as indicated by a curve progression being parallel to the abscissa, maximum magnetization M_{7T} of the samples was measured at $B = 7$ T. It is distinguishable that the addition of Ga:Fe$_2$O$_3$ NCs leads to a proportional increase of coercive field H_c, maximum magnetization at $B = 7$ T M_{7T}, and remanence M_R of the blended material. The coercive field H_c of the cement-nanocrystal mixtures increases from $H_c = 10$ mT (non-blended hard-
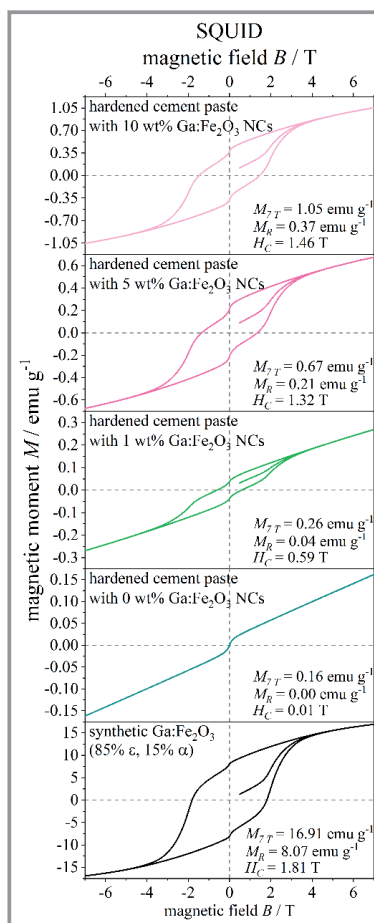
lus M_{IT} show only minor differences, whereby the latter is dependent on the material's stiffness. Its respective median decreases slightly from approximately 23 to 20 kN mm^{-2}, while overall distribution width increases from approximately ±2 to ±3 kN mm^{-2} (Fig. 6a,b). Hardly any changes are visible for the nano indentation hardness H_{IT} and modulus M_{IT} (Fig. 6c,d), where median values and distribution widths remain the same. The size of nano additive Ga:Fe$_2$O$_3$ (22 nm ± 11 nm) is rather small compared to the volumes probed by nano-indentation, i.e., penetration depth of 250 nm, and no impact on the micro-scale mechanics arises. The same applies to micro-indentation with a penetration depth of 24 µm.

It can be concluded that an increasing mass fraction of Ga:Fe$_2$O$_3$ NCs leads to a loss in macroscopic strength, while the mechanical properties (hardness and stiffness) on the micro- and nano-scale hardly change. Therefore, loss in mechanical strength seems to arise from increased porosity rather than alteration of cement paste's matrix incorporating Ga:Fe$_2$O$_3$ NCs.

3.2.2 Magnetic Properties

To appraise the magnetic character of hardened cement paste mixed with different mass fractions of Ga:Fe$_2$O$_3$ NCs, SQUID measurements were conducted (Fig. 7), where the magnetic moment M was measured against an external magnetic field $\vec{H}$ in a range of -7 T $\leq B \leq 7$ T and evaluated regarding the maximum magnetization at $B = 7$ T M_{7T}, remanence M_R, and coercive field H_C.

Figure 7. SQUID data of hardened cement paste s mixed with different mass fractions of Ga:Fe$_2$O$_3$ NCs measured at 27 °C in an external field $\vec{H}$ of -7 T $\leq B \leq 7$ T with $B'(t) = 5$ Oe s^{-1}; with $H_c \equiv$ coercive field, $M_R \equiv$ remanence, and $M_{7T} \equiv$ maximum magnetization at $B = 7$ T.

Online in color, print in grayscale unless the author(s) contribute to the costs.
✓✓ **These are not the final page numbers!**

6

Research Article

Chemie
Ingenieur
Technik

ened cement paste) to $H_c = 1.46$ T (blended with 10 wt % Ga:Fe$_2$O$_3$ NCs), which is relatively close to that of the pure nanocrystals ($H_c = 1.81$ T). A possible explanation for this might be a magnetic exchange bias between the nanocrystal grains and the cement matrix. Due to the high magnetocrystalline anisotropy of Ga:Fe$_2$O$_3$ NCs, the nanocrystal grains keep their magnetic moment M undirected to the external magnetic field $\vec{H}$, increasing the energy needed to align the spins of the surrounding matrix (Fig. 8). We assume that, by lowering the external magnetic field $\vec{H}$, at first only the spins of the cement matrix furthest away from the NCs de-align and at an external magnetic field $\vec{H} \cong 0$ T only the NCs are still fully aligned. To achieve the ground state, a negative external magnetic field $\vec{H}$ has to be applied.

In the case of maximum magnetization at $B = 7$ T M_{7T}, the sample with the highest mass fraction (10 wt %) exhibits only approximately 6 % of maximum magnetization at $B = 7$ T M_{7T} of the native Ga:Fe$_2$O$_3$ NCs, while the coercive field H_c is approximately 81 %, which is attributed to the lower amounts of unpaired electron spins per mole. Further, the remanence M_R of the blended hardened cement paste samples increases linearly with the added amount of Ga:Fe$_2$O$_3$ NCs. At the same time, the remanence M_R value normalized by the magnetic mass ($M_R = 3.9$ emu g^{-1} ± 0.3 emu g^{-1}) is in all cases half of the synthetic Ga:Fe$_2$O$_3$ NCs ($M_R = 8.07$ emu g^{-1}) probably due to the interaction with the cement matrix (Figs. 7 and 8).

In summary, the addition of different mass fractions (1–10 wt %) of Ga:Fe$_2$O$_3$ NCs enhanced coercive field H_c, maximum magnetization at $B = 7$ T M_{7T}, and remanence M_R compared to pure hardened cement paste, wherein the extrapolated remanence M_R was approximately half of the native Ga:Fe$_2$O$_3$ NCs'. This effect was attributed to the interaction between the electron spins of residue calcium aluminum ferrite (brownmillerite, C$_4$AF) with a low coercive field H_c and the electron spins of Ga:Fe$_2$O$_3$ with strong magnetic anisotropy. Cement seems to be a good matrix to isolate the Ga:Fe$_2$O$_3$ NCs, although halving the remanence M_R while not interfering with their maximum magnetization at $B = 7$ T M_{7T}.

Figure 8. Scheme of alignment of the magnetic moment M in hardened cement pastes mixed with Ga:Fe$_2$O$_3$ NCs in an external field $\vec{H}$ of -7 T $\leq B \leq 7$ T.

– The higher the Ga:Fe$_2$O$_3$ content, the higher the porosity and, consequently, the lower the sample density.
– Coercive field H_C and magnetic remanence M_R are proportionally enhanced with rising Ga:Fe$_2$O$_3$ content, while the maximum magnetization at $B = 7$ T M_{7T} was only slightly affected.
– Micro- and nanoscale mechanical properties remain unaffected, no matter how much Ga:Fe$_2$O$_3$ is added, while compressive strength decreases.

In this work, we showed how and to which extent the amount of Ga:Fe$_2$O$_3$ NCs influences properties relevant to the practice of hardened cement paste, hence also the concrete properties, using a cheap and easily mass-producible nanoscale additive. The shown properties of blended hardened cement paste might make it a promising material for coatings of facades or interior walls, when it comes to niche applications like the demand for protection against wireless eavesdropping. Implementing these properties into concrete might enable constructions to protect sensitive machinery that is negatively influenced by radio waves, like magnetic resonance tomography in the medical field, to ensure greater lifetime and efficiency. At the same time, sensitive data can be protected by blocking the external access from third parties, i.e., enhanced tap-proofness or protection against wireless eavesdropping, but this will be in focus of investigation of future works.

4 Conclusion

Hardened cement pastes were prepared from a standard Portland cement (CEM I 42.5R) and different amounts of hard magnetic nanocrystals, and their structure-property relationships have been tested. Decisive physical properties of hardened cement paste were affected by the addition of this type of NCs:
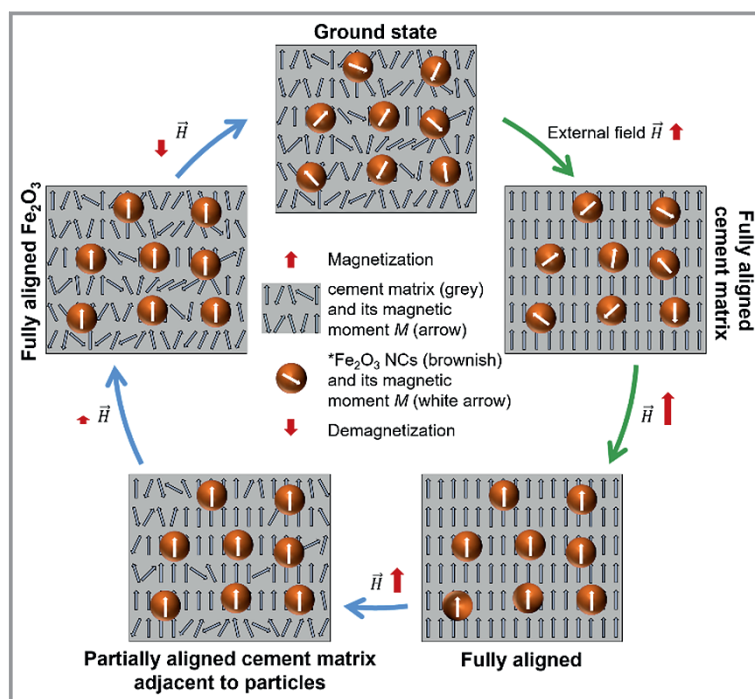
www.cit-journal.com

© 2023 The Authors. Chemie Ingenieur Technik published by Wiley-VCH GmbH

Chem. Ing. Tech. **2023**, *95*, No. 00, 1–10

Supporting Information

Supporting Information for this article can be found under DOI: https://doi.org/10.1002/cite.202300022. This document includes all experimental procedures, additional measurements as well as additional references to primary literature relevant for this study [43–80].

Acknowledgment

Symbols used

A	[–]	damping constant
B	[T, or 10^5 Oe]	magnetic field
$B'(t)$	[Oe s^{-1}]	alteration rate of magnetic field
C_C	[mm]	lenses' chromatic aberration in TEM
C_S	[mm]	lenses' spherical aberration in TEM
d	[m]	diameter
d_{10}	[m]	10 % are below this diameter
d_{50}	[m]	50 % are below this diameter or median
d_{90}	[m]	90 % are below this diameter or 10 % above
d_{pore}	[m]	pore size
d_{shaft}	[m]	diameter of mixing shaft
$\bar{d}$	[m]	mean diameter or average diameter
$\bar{d}_{pore}$	[m]	mean pore size or average pore size
$d\Delta m/(dt)$	[wt % h^{-1}]	time derived weight loss in TGA
E	[–]	effective demagnetization factor
f_{ck}	[N mm^{-2}]	compressive strength
f_r	[s^{-1}]	resonance frequency
$\vec{H}$	[T]	external magnetic field
H_a	[T]	uniaxial anisotropy field of the unpatterned film
H_C	[T]	coercive field
H_{IT}	[N mm^{-2}]	hardness of indentation
$I_{reflection}$	[–]	intensity of reflection in XRD
M	[emu g^{-1}]	magnetic moment
M_{7T}	[emu g^{-1}]	maximal magnetization at $B = 7$ T
M_{IT}	[N mm^{-2}]	modulus of indentation
M_R	[emu g^{-1}]	remanence
p	[10^5 Pa]	pressure
p/p_0	[–]	relative pressure for nitrogen physisorption
p_{intr}	[10^8 Pa]	pressure of intrusion for Hg-porosimetry
$\dot{s}$	[mm s^{-1}]	velocity
T_{ref}	[°C]	reference temperature
V	[mL]	volume
V_p	[µL]	pore volume
$V_{p,total}$	[µL]	total pore volume
V_{sample}	[µL]	sample volume
w/c	[–]	gravimetric water to cement ratio

Greek letters

α	[–]	crystal phase
γ	[T^{-1}s^{-1}]	gyromagnetic ratio; $1.76 \cdot 10^{11}$
δ	[°]	contact angle
ε	[–]	crystal phase
η	[N m^{-1}]	surface tension
θ	[°]	annular position of source and detector in XRD, relative to sample

Abbreviations

AR	aspect ratio
BET	Brunauer-Emmert-Teller
BJH	Barrett-Joyner-Halenda
C-S-H	calcium silicate hydrate; m CaO · SiO$_2$ · n H$_2$O
DFT	density functional theory
eq.	equivalent
EDXS	energy-dispersive X-ray spectroscopy
Ga:Fe$_2$O$_3$	gallium substituted iron oxide [Ga$_{0.043}$Fe$_{1.957}$O$_3$]
NC	nanocrystals
rcf	relative centrifugal force
SEM	scanning electron microscopy
SQUID	superconducting quantum interference device
TEM	transmission electron microscopy
TGA	thermogravimetric analysis
XRD	X-ray diffraction

References

[1] J. Rieger, M. Kellermeier, L. Nicoleau, *Angew. Chem., Int. Ed.* **2014**, *53* (46), 12380–12396. DOI: https://doi.org/10.1002/anie.201402890

[2] DIN EN 197-1:2011-11, *Cement – Part 1: Composition, Specifications and Conformity Criteria for Common Cements; German Version EN 197-1:2011*, Beuth Verlag, Berlin **2011**.

[3] E. D. Hondros, E. Bullock, *Angew. Chem., Int. Ed.* **1989**, *28 (8)*, 1088–1097. DOI: https://doi.org/10.1002/anie.198910881

[4] *Zement-Taschenbuch*, Vol. 50, Verein Deutscher Zementwerke e.V., Düsseldorf **2002**.

[5] H. Moosberg-Bustnes, B. Lagerblad, E. Forssberg, *Mater. Struct.* **2004**, *37 (2)*, 74–81. DOI: https://doi.org/10.1007/bf02486602

[6] *Blast Furnace Slag*, Federal Highway Administration, U.S. Department of Transportation, Washington, DC **2007**. https://www.fhwa.dot.gov/publications/research/infrastructure/pavements/97148/010.cfm

[7] *Chapter 3 – Fly Ash in Portland Cement Concrete*, in *Fly Ash Facts for Highway Engineers*, Federal Highway Administration, U.S. Department of Transportation, Washington, DC **2007**. https://www.fhwa.dot.gov/pavement/recycling/fach03.cfm

[8] *Silica Fume User's Manual*, Federal Highway Administration, U.S. Department of Transportation, Washington, DC **2007**, 1–194. https://silicafume.org/concrete-manual.html

[9] T. R. S. Mullapudi, D. Gao, A. Ayoub, *Mag. Concr. Res.* **2013**, *65 (18)*, 1081–1091. DOI: https://doi.org/10.1680/macr.12.00187

[10] H. E. Elyamany, A. E. M. Abd Elmoaty, B. Mohamed, *Alexandria Eng. J.* **2014**, *53 (2)*, 295–307. DOI: https://doi.org/10.1016/j.aej.2014.03.010

[11] S. H. Kosmatka, B. Kerkhoff, W. C. Panarese, *Design and Control of Concrete Mixtures*, 14th ed., Portland Cement Association, Washington, DC **2008**.

[12] C. Y. Tuan, S. Yehia, *Aci Mater. J.* **2004**, *101*, 287–293.

[13] E. A. Avallone, T. B. Iii, *Marks' Standard Handbook for Mechanical Engineers*, Vol. 34, McGraw Hill, New York **1997**.

[14] D. Feng, N. Xie, C. Gong, Z. Leng, H. Xiao, H. Li, X. Shi, *Ind. Eng. Chem. Res.* **2013**, *52 (33)*, 11575–11582. DOI: https://doi.org/10.1021/ie4011595

[15] L. Senff, D. M. Tobaldi, P. Lemes-Rachadel, J. A. Labrincha, D. Hotza, *Constr. Build. Mater.* **2014**, *65*, 191–200. DOI: https://doi.org/10.1016/j.conbuildmat.2014.04.121

[16] S. A. Ghahari, E. Ghafari, N. Lu, *Constr. Build. Mater.* **2017**, *146*, 755–763. DOI: https://doi.org/10.1016/j.conbuildmat.2017.04.165

[17] R. Siddique, A. Mehta, *Constr. Build. Mater.* **2014**, *50*, 116–129. DOI: https://doi.org/10.1016/j.conbuildmat.2013.09.019

[18] M. Ghosal, A. K. Chakraborty, *Adv. Polym. Mater. Synth. Appl.* **2018**, *July*, 121–142.

[19] M. Heikal, *J. Therm. Anal. Calorim.* **2016**, *126 (3)*, 1077–1087. DOI: https://doi.org/10.1007/s10973-016-5715-0

[20] M. Heikal, M. E. A. Zaki, S. M. Ibrahim, *Constr. Build. Mater.* **2021**, *269*, 121310. DOI: https://doi.org/10.1016/j.conbuildmat.2020.121310

[21] H. Li, H. Xiao, J. Yuan, J. Ou, *Compos. Part B Eng.* **2004**, *35 (2)*, 185–189. DOI: https://doi.org/10.1016/S1359-8368(03)00052-0

[22] H. Li, H. Xiao, J. Ou, *Cem. Concr. Res.* **2004**, *34 (3)*, 435–438. DOI: https://doi.org/10.1016/j.cemconres.2003.08.025

[23] M. H. Zhang, J. Islam, *Constr. Build. Mater.* **2012**, *29*, 573–580. DOI: https://doi.org/10.1016/j.conbuildmat.2011.11.013

[24] K. J. Krakowiak, J. J. Thomas, S. Musso, S. James, A.-T. Akono, F.-J. Ulm, *Cem. Concr. Res.* **2015**, *67*, 103–121. DOI: https://doi.org/10.1016/j.cemconres.2014.08.008

[25] M. S. El-Feky, P. Youssef, A. M. El-Tair, S. Ibrahim, M. Serag, *AIMS Mater. Sci.* **2019**, *6 (6)*, 864–883. DOI: https://doi.org/10.3934/matersci.2019.6.864

[26] B. B. Mukharjee, S. V. Barai, *Constr. Build. Mater.* **2014**, *68*, 416–425. DOI: https://doi.org/10.1016/j.conbuildmat.2014.06.074

[27] D. Kong, H. Zhang, X. Du, Y. Yang, S. P. Shah, S. Wei, *Constr. Build. Mater.* **2012**, *37*, 707–715. DOI: https://doi.org/10.1016/j.conbuildmat.2012.08.006

[28] M. Diez-Garcia, J. J. Gaitero, J. S. Dolado, C. Aymonier, *Angew. Chem., Int. Ed.* **2017**, *56 (12)*, 3162–3167. DOI: https://doi.org/10.1002/anie.201611858

[29] S. Ohkoshi, S. Kuroki, S. Sakurai, K. Matsumoto, K. Sato, S. Sasaki, *Angew. Chem., Int. Ed.* **2007**, *46 (44)*, 8392–8395. DOI: https://doi.org/10.1002/anie.200703010

[30] S. J. Barnett, *Rev. Mod. Phys.* **1935**, *7 (2)*, 129–166. DOI: https://doi.org/10.1103/RevModPhys.7.129

[31] C. Kittel, *Phys. Rev.* **1948**, *73 (2)*, 155–161. DOI: https://doi.org/10.1103/PhysRev.73.155

[32] K. Kelml, W. Maderl, *Z. Anorg. Allg. Chem.* **2005**, *631 (12)*, 2383–2389. DOI: https://doi.org/10.1002/zaac.200500283

[33] M. Thommes, K. Kaneko, A. V. Neimark, J. P. Olivier, F. Rodriguez-Reinoso, J. Rouquerol, K. S. W. Sing, *Pure Appl. Chem.* **2015**, *87 (9–10)*, 1051–1069. DOI: https://doi.org/10.1515/pac-2014-1117

[34] *Ultrafeine Aerosole und Nanopartikel am Arbeitsplatz*, Deutsche Gesetzliche Unfallversicherung, Berlin. https://www.dguv.de/ifa/fachinfos/nanopartikel-am-arbeitsplatz/index.jsp

[35] E. W. Washburn, *Phys. Rev.* **1921**, *17 (3)*, 273–283. DOI: https://doi.org/10.1103/PhysRev.17.273

[36] DIN ISO 15901-1:2019-03, *Evaluation of Pore Size Distribution and Porosity of Solid Materials by Mercury Porosimetry and Gas Adsorption – Part 1: Mercury Porosimetry (ISO 15901-1:2016)*, Beuth Verlag, Berlin **2019**.

[37] DIN EN 12390-3:2019-10, *Testing Hardened Concrete – Part 3: Compressive Strength of Test Specimens; German Version EN 12390-3:2019*, Beuth Verlag, Berlin **2019**.

[38] D. Neumannl, U. Weinbrennerl, U. Hestermannl, L. Rongenl, *Frick/Knöll Baukonstruktionslehre 2*, Vieweg+Teubner Verlag, Wiesbaden **2003**.

[39] W. Oliver, G. Pharr, *J. Mater. Res.* **1992**, *7 (6)*, 1564–1583.

[40] L. Khanna, N. K. Verma, *J. Magn. Magn. Mater.* **2013**, *336*, 1–7. DOI: https://doi.org/10.1016/j.jmmm.2013.02.016

[41] Z. C. Lu et al., *Data Br.* **2019**, *27*, 104699. DOI: https://doi.org/10.1016/j.dib.2019.104699

[42] F. D. Tamás, A. Vértes, *Cem. Concr. Res.* **1973**, *3 (5)*, 575–581. DOI: https://doi.org/10.1016/0008-8846(73)90095-1

[43] DFG SPP 2005, *Priority Programm "Opus Fluidum Futurum – Rheology of Reactive, Multiscale, Multiphase Construction Materials"*, **2018**. www.spp2005.de/

[44] H. M. Rietveld, *J. Appl. Crystallogr.* **1969**, *2 (2)*, 65–71. DOI: https://doi.org/10.1107/S0021889869006558

[45] P. Paufler, *Cryst. Res. Technol.* **1995**, *30 (4)*, 494–494. DOI: https://doi.org/10.1002/crat.2170300412

[46] F. Nishi, Y. Takéuchi, *Acta Crystallogr.* **1975**, *B31 (4)*, 1169–1173. DOI: https://doi.org/10.1107/S0567740875004736

[47] A. A. Colville, S. Geller, *Acta Crystallogr.* **1971**, *B27 (12)*, 2311–2315. DOI: https://doi.org/10.1107/s056774087100579x

[48] Q. Huang, O. Chmaissem, J. J. Capponi, C. Chaillout, M. Marezio, J. L. Tholence, A. Santoro, *Physica C* **1994**, *227 (1–2)*, 1–9. DOI: https://doi.org/10.1016/0921-4534(94)90349-2

[49] J. C. A. Boeyens, V. V. H. Ichharam, *Z. Kristallogr. – New Cryst. Struct.* **2002**, *217*, 9–10. DOI: https://doi.org/10.1524/ncrs.2002.217.jg.9

[50] L. Desgranges, D. Grebille, G. Calvarin, G. Chevrier, N. Floquet, J. -C Niepce, *Acta Crystallogr., Sect. B: Struct. Sci.* **1993**, *49 (5)*, 812–817. DOI: https://doi.org/10.1107/S0108768193003556

[51] G. A. Lager, J. D. Jorgensen, F. J. Rotella, *J. Appl. Phys.* **1982**, *53 (10)*, 6751–6756. DOI: https://doi.org/10.1063/1.330062

[52] M. R. Hartman, R. Berliner, *Cem. Concr. Res.* **2006**, *36 (2)*, 364–370. DOI: https://doi.org/10.1016/j.cemconres.2005.08.004

[53] M. I. McCarthy, N. M. Harrison, *Phys. Rev. B* **1994**, *49 (13)*, 8574–8582. DOI: https://doi.org/10.1103/PhysRevB.49.8574

[54] T. Pilati, F. Demartin, C. M. Gramaccioli, *Acta Crystallogr., Sect. B Struct. Sci.* **1998**, *54 (5)*, 515–523. DOI: https://doi.org/10.1107/S0108768197018181

[55] Á. G. De La Torre, S. Bruque, J. Campo, M. A. G. Aranda, *Cem. Concr. Res.* **2002**, *32 (9)*, 1347–1356. DOI: https://doi.org/10.1016/S0008-8846(02)00796-2

[56] F. C. Hawthorne, R. B. Ferguson, *Can. Mineral.* **1975**, *13*, 289–292.

[57] J. A. McGinnety, *Acta Crystallogr., Sect. B Struct. Crystallogr. Cryst. Chem.* **1972**, *28 (9)*, 2845–2852. DOI: https://doi.org/10.1107/s0567740872007022

[58] C. Bezou, A. Nonat, J.-C. Mutin, A. N. Christensen, M. S. Lehmann, *J. Solid State Chem.* **1995**, *117 (1)*, 165–176. DOI: https://doi.org/10.1006/jssc.1995.1260

[59] W. Mumme, R. Hill, G. Bushnellwye, E. Segnit, *Neues Jahrb. Mineral.* **1995**, *169 (1)*, 35–68.

[60] P. Mondal, J. W. Jeffery, *Acta Crystallogr., Sect. B Struct. Crystallogr. Cryst. Chem.* **1975**, *31 (3)*, 689–697. DOI: https://doi.org/10.1107/S0567740875003639

[61] S. Brunauer, P. H. Emmett, E. Teller, *J. Am. Chem. Soc.* **1938**, *60 (2)*, 309–319. DOI: https://doi.org/10.1021/ja01269a023

[62] R. M. Dreizler, E. K. U. Gross, in *Density Funct. Theory*, Springer, Heidelberg **1990**.

[63] L. D. Gelb, K. E. Gubbins, R. Radhakrishnan, M. Sliwinska-Bartkowiak, *Rep. Prog. Phys.* **1999**, *62*, 1573–1659. DOI: https://doi.org/10.1088/0034-4885/77/5/056502

[64] *NOVA®-e Series Models 25 and 26 NovaWin/NovaWin-CFR*, Operating Manual, Version 11.01/11.02, Quantachrome Instruments, Boynton Beach, FL **2012**, 124–126. https://dokumen.tips/documents/gas-sorption-system-operating-manual.html?page=124

[65] E. P. Barrett, L. G. Joyner, P. P. Halenda, *J. Am. Chem. Soc.* **1951**, *73 (1)*, 373–380. DOI: https://doi.org/10.1021/ja01145a126

[66] T. J. Mays, *Stud. Surf. Sci. Catal.* **2007**, *160*, 57–62. DOI: https://doi.org/10.1016/s0167-2991(07)80009-7

[67] *A Practical Guide to Microstructural Analysis of Cementitious Materials* (Eds: K. Scrivener, R. Snellings, B. Lothenbach), CRC Press, Boca Raton, FL **2015**.

[68] Q, Yu, H. J. H. Brouwers, in *Proc. 8th fib Int. PhD Symposium in Civil Engineering* (Eds: G. Fischer, M. Geiker, O. Hededa, L. Ottoson, H. Stang), Technical University of Denmark, Lyngby **2010**.

[69] C. G. Vassileva, S. V. Vassilev, *Fuel Process. Technol.* **2005**, *86 (12–13)*, 1297–1333. DOI: https://doi.org/10.1016/j.fuproc.2005.01.024

[70] J. Dweck, P. M. Buchler, A. C. V. Coelho, F. K. Cartledge, *Thermochim. Acta* **2000**, *346 (1–2)*, 105–113. DOI: https://doi.org/10.1016/S0040-6031(99)00369-X

[71] D. J. Morgan, *Clay Miner.* **1978**, *13 (1)*, 132–132. DOI: https://doi.org/10.1180/claymin.1978.013.1.11

[72] A. Bakolas, E. Aggelakopoulou, A. Moropoulou, *J. Therm. Anal. Calorim.* **2008**, *92 (1)*, 345–351. DOI: https://doi.org/10.1007/s10973-007-8858-1

[73] K. Wang, S. P. Shah, A. Mishulovich, *Cem. Concr. Res.* **2004**, *34 (2)*, 299–309. DOI: https://doi.org/10.1016/j.cemconres.2003.08.003

[74] R. Zboril, M. Mashlan, D. Petridis, *Chem. Mater.* **2002**, *14 (3)*, 969–982. DOI: https://doi.org/10.1021/cm0111074

[75] E. Tronc, C. Chanéac, J. P. Jolivet, *J. Solid State Chem.* **1998**, *139 (1)*, 93–104. DOI: https://doi.org/10.1006/jssc.1998.7817

[76] H. Tokoro, W. Tarora, A. Namai, M. Yoshikiyo, S. Ohkoshi, *Chem. Mater.* **2018**, *30 (9)*, 2888–2894. DOI: https://doi.org/10.1021/acs.chemmater.7b03708

[77] A. Namai et al., *Nat. Commun.* **2012**, *3 (1)*, 1035. DOI: https://doi.org/10.1038/ncomms2038

[78] C. Jakob, D. Jansen, N. Ukrainczyk, E. Koenders, U. Pott, D. Stephan, J. Neubauer, *Materials (Basel)* **2019**, *12 (18)*, 2957. DOI: https://doi.org/10.3390/ma12182957

[79] C. Jakob, D. Jansen, U. Pott, J. Neubauer, Comparing Phase Development and Rheological Properties of OPC Paste Within the First Hour of Hydration, in *Rheology and Processing of Construction Materials* (Eds: V. Mechtcherine, K. Khayat, E. Secrieru), vol. 23, Springer, Cham **2019**. DOI: https://doi.org/10.1007/978-3-030-22566-7_26

[80] P. A. Kißling et al., *Constr. Build. Mater.*, submitted.

Online in color, print in grayscale unless the author(s) contribute to the costs.
✓✓ These are not the final page numbers!

10

Research Article

Chemie Ingenieur Technik

Impact of Hard Magnetic Nanocrystals on the Properties of Hardened Cement Paste

Patrick A. Kißling, Markus Mahlbacher, Christoph Wesemann, Alexander Mundstock, Franziska Lübkemann-Warwas, Stephen Klimke, Franz Renz, Ludger Lohaus, Michael Haist, Nadja C. Bigall*

Research Article: The impact of different amounts of incorporated hard magnetic $Ga_{0.043}Fe_{1.957}O_3$ (85 % ε and 15 % α phase) nanocrystals (NCs) on the physical properties of hardened cement paste is shown. By adding these Fe_2O_3 NCs it is possible to modify the manifold properties simultaneously, thus, enabling fine-tuned buildings or coatings. ...... ■